TrackCraft3R: Repurposing Video Diffusion Transformers for Dense 3D Tracking

Jisu Nam[1] **Jahyeok Koo**[1] **Soowon Son**[1] **Jaewoo Jung**[1]
Honggyu An[1] **Junhwa Hur**[2†] **Seungryong Kim**[1†]

[1]KAIST AI [2]Google DeepMind

https://cvlab-kaist.github.io/TrackCraft3r

Abstract

Dense 3D tracking from monocular video is fundamental to dynamic scene understanding. While recent 3D foundation models provide reliable per-frame geometry, recovering object motion in this geometry remains challenging and benefits from strong motion priors learned from real-world videos. Existing 3D trackers either follow iterative paradigms trained from scratch on synthetic data or fine-tune 3D reconstruction models learned from static multi-view images, both lacking real-world motion priors. Pre-trained video diffusion transformers (video DiTs) offer rich spatio-temporal priors from internet-scale videos, making them a promising foundation for 3D tracking. However, their *frame-anchored* formulation, which generates each frame's content, is fundamentally mismatched with *reference-anchored* dense 3D tracking, which must follow the same physical points from a reference frame across time. We present TrackCraft3R, the first method to repurpose a video DiT as a feed-forward dense 3D tracker. Given a monocular video and its frame-anchored reconstruction pointmap, TrackCraft3R predicts a reference-anchored tracking pointmap that follows every pixel of the first frame across time in a single forward pass, along with its visibility. We achieve this through two designs: (i) a *dual-latent representation* that uses per-frame geometry latents and reference-anchored track latents as dense queries, and (ii) *temporal RoPE alignment*, which specifies the target timestamp of each track latent. Together, these designs convert the per-frame generative paradigm of video DiTs into a reference-anchored tracking formulation with LoRA fine-tuning. TrackCraft3R achieves state-of-the-art performance on standard sparse and dense 3D tracking benchmarks, while running $1.3\times$ faster and using $4.6\times$ less peak memory than the strongest prior method. We further demonstrate robustness to large motions and long videos.

1 Introduction

Recovering dense 3D trajectories from monocular video [7, 13, 55, 70, 76] is a fundamental building block for robotic manipulation [2, 38], dynamic scene reconstruction [17, 45], and controllable video generation [15, 53]. Because apparent motion is often dominated by camera ego-motion rather than object motion, accurate tracking requires reasoning in a 3D world coordinate frame in which camera motion is canceled out. Recent advances in monocular depth and pose estimation [18, 25, 44, 46] now provide reliable 3D geometry for arbitrary videos, enabling 3D trackers [55, 76, 84] to operate in a world coordinate frame where only residual object motion remains to be recovered.

Early 3D trackers [54, 55, 70, 75, 76] follow the 2D tracker paradigm such as CoTracker paradigm [33, 34], which iteratively updates trajectories based on local 3D correlation features, and is trained from

[†]Co-corresponding.

scratch on synthetic 4D datasets [16, 32, 86]. More recent feed-forward approaches [13, 35, 49, 65] instead fine-tune pre-trained 3D reconstruction models [37, 42, 72]. While their pre-trained models offer strong spatial priors, they are learned from static multi-view images, lack rich temporal priors from real-world videos.

On the other hand, recent works demonstrate that pre-trained video diffusion models [3, 77], especially video diffusion transformers (DiTs) [40, 69, 81], already encode strong spatio-temporal priors from internet-scale real videos and effectively transfer to perception tasks such as video depth [24, 62, 85], camera pose [29], and pointmap estimation [51].

This motivates a key question: *can we leverage the spatio-temporal priors of video DiTs for dense 3D tracking?* This is challenging because existing diffusion-based perception models produce *frame-anchored* outputs (*i.e.*, predictions defined independently at each frame [24, 29, 51, 62, 85]), whereas dense 3D tracking requires *reference-anchored* representations (*i.e.*, tracking the same physical points from a reference frame across time). A concurrent work, MotionCrafter [87], repurposes a video diffusion U-Net [3] for 4D reconstruction, but predicts *frame-anchored* scene flow between adjacent frames, requiring temporal chaining for dense 3D tracking and potentially leading to error accumulation, especially under occlusion.

In this paper, we introduce **TrackCraft3R**, the first method that repurposes a video diffusion transformer [69] as a feed-forward dense 3D tracker. Given a monocular video and its *frame-anchored* reconstruction pointmap in world coordinates [25, 44, 46], TrackCraft3R predicts, in a single forward pass, a *reference-anchored* tracking pointmap that tracks every pixel in the first frame across time, along with its visibility.

We achieve this by repurposing two core components of the video DiTs. First, we introduce a **dual-latent representation** consisting of (i) *geometry latents*, which encode each frame's RGB and reconstruction pointmap, and (ii) *first-frame anchored track latents*, which encode the reference frame's RGB and pointmap. The track latents act as dense query points defined in the first frame, while geometry latents represent 3D geometry over time in a shared world coordinate frame. Through full 3D attention, each track latent attends to geometry latents across frames to determine *where* its corresponding point is and *what* 3D position it should take. Second, we propose a **temporal RoPE alignment**, repurposing rotary positional embedding (RoPE) [64] to encode the target timestamp of each track latent, specifying *when* it attends to geometry latents. Together, TrackCraft3R enables dense 3D tracking with LoRA [23] fine-tuning, effectively converting the per-frame generative paradigm of video DiTs into a reference-anchored dense tracking paradigm.

TrackCraft3R achieves state-of-the-art performance on standard 3D sparse and dense tracking benchmarks [16, 31, 32, 41, 56, 86]. Notably, TrackCraft3R runs $1.3\times$ faster and uses $4.6\times$ less peak memory than the state-of-the-art 3D tracker DELTAv2 [55]. We further demonstrate robustness to large motions and long videos, and extensive ablations validate our design choices.

In summary, our contributions are threefold: (1) we present **TrackCraft3R**, the first method to repurpose a video diffusion transformer for feed-forward dense 3D tracking; (2) we propose a dual-latent representation and temporal RoPE alignment to convert frame-anchored generation into first-frame-anchored dense 3D tracking; and (3) we achieve state-of-the-art performance on standard 3D tracking benchmarks, while demonstrating robustness to large temporal strides and long videos.

2 Related Work

3D Point Tracking. Point tracking aims to recover long-range motion trajectories in videos. Early 2D tracking methods [6, 11, 12, 19, 33, 34, 60] iteratively refine trajectories within sliding temporal windows. To extend this to 3D, several works incorporate monocular depth [46, 80] and track in camera coordinates [54, 55, 70, 75], while others [76, 84] further utilize camera poses [25, 44, 46] to operate in a world coordinate frame, where camera motion is explicitly compensated. However, these methods rely on iterative trajectory updates and are trained from scratch on synthetic 4D datasets [16, 32, 86].

Recent feed-forward approaches [13, 17, 30, 35, 45, 49, 65] instead propose to fine-tune pre-trained 3D reconstruction models [37, 42, 72, 79] on synthetic 4D data. While these methods benefit from strong spatial priors of pre-trained models, they still lack strong temporal priors from real-world video dynamics. A concurrent work, MotionCrafter [87], incorporates temporal priors by

repurposing a video diffusion U-Net [3] for 4D reconstruction. However, it predicts frame-anchored scene flow between adjacent frames, requiring temporal chaining that accumulates errors under occlusion. In contrast, TrackCraft3R repurposes a video diffusion transformer to directly produce reference-anchored tracking pointmap in a single forward pass, avoiding temporal chaining.

Video Diffusion Models for Frame-Anchored Perception. Image diffusion models have been successfully repurposed for a wide range of perception tasks, including depth estimation [21, 36], surface normal prediction [14, 21], dense correspondence [22, 52, 68], and optical flow [61]. This paradigm has naturally extended to the video domain, where video diffusion models provide robust spatio-temporal priors. Early works repurpose video diffusion U-Nets [3, 77] for temporally consistent video depth estimation [24, 62], per-frame pointmap estimation [78], and joint estimation of depth, pointmaps, and ray maps [29]. Recently video diffusion transformers (DiTs) [40, 69, 81] has driven performance improvement across multiple tasks: DVD [85] repurposes the Wan 2.1 DiT [69] for video depth, and Sora3R [51] adapts an OpenSora DiT for pointmap prediction.

Despite the diversity of tasks, all these methods produce frame-anchored outputs, where predictions are tied to the content and timestamp of individual frames. Dense 3D tracking, by contrast, requires reference-anchored predictions that follow the same physical content from a reference frame across time. To the best of our knowledge, TrackCraft3R is the first to repurpose a video DiT for reference-anchored dense 3D tracking. A recent work [63] leverages video DiT features for sparse 2D point tracking. However, this method adds a tracking head (*e.g.*, a CoTracker head [34]) on top of the video DiT features, rather than repurposing the video DiT itself.

3 Preliminaries

Variational Autoencoder (VAE). A VAE encoder $\mathcal{E}$ maps a video $\mathbf{V} \in \mathbb{R}^{(1+F)\times H\times W\times 3}$ into a latent representation $\mathbf{z} = \mathcal{E}(\mathbf{V}) \in \mathbb{R}^{(1+f)\times h\times w\times c}$, where H, W, and $(1+F)$ denote the spatial resolution and number of frames, and h, w, and $(1+f)$ denote their spatially and temporally downsampled counterparts. c is the latent channel dimension. Here, temporal downsampling is applied only to the F frames, while the first frame is preserved. A decoder $\mathcal{D}$ reconstructs the video from $\mathbf{z}$.

Prior works show that VAEs pre-trained on RGB videos can be repurposed to encode and decode geometric modalities such as pointmaps [51, 78], depth maps [24, 85], and camera rays [28, 29], enabling diffusion models to operate in this latent space for geometric prediction.

Video Diffusion Transformers (DiTs). The latent $\mathbf{z}$ is patchified and projected, and a transformer f_θ is trained with rectified flow matching [48] to predict the velocity field along a linear interpolation between noise and data. The model applies full 3D attention, where each token i produces query $\mathbf{q}_i$, key $\mathbf{k}_i$, and value $\mathbf{v}_i$, and attends to all the other tokens j with weights proportional to $\mathbf{q}_i^\top \mathbf{k}_j/\sqrt{d_k}$, where d_k is the key dimension.

In this work, following [21, 85], we repurpose f_θ as a feed-forward regressor rather than a multi-step denoiser, enabling efficient inference without iterative sampling.

3D Rotary Positional Embedding (3D RoPE). To encode relative spatio-temporal structure, video DiTs employ 3D RoPE [64]. The channel dimension of each query and key vector is partitioned into temporal and spatial groups, and axis-specific rotation matrices are applied on each token's 3D position $\mathbf{p}_i = (x_i, y_i, t_i)$, where (x_i, y_i) denote spatial coordinates and t_i denotes the temporal index. Under RoPE, the attention score between tokens i and j becomes

$$\tilde{\mathbf{q}}_i^\top \tilde{\mathbf{k}}_j = \mathbf{q}_i^\top \mathbf{R}_{\mathbf{p}_j - \mathbf{p}_i} \mathbf{k}_j, \tag{1}$$

where $\tilde{\mathbf{q}}_i$ and $\tilde{\mathbf{k}}_j$ denote the query and key vectors after applying RoPE. $\mathbf{R}_{\mathbf{p}_j-\mathbf{p}_i}$ is a block-diagonal rotation matrix parameterized by the relative offset $\mathbf{p}_j - \mathbf{p}_i$. Thus, attention depends only on relative positions, *i.e.*, tokens with similar t_i interact more strongly.

4 Video Diffusion Transformer for Dense 3D Tracking

We present a novel framework that densely tracks dynamic video content in a 3D world coordinate frame in a single forward pass. Recent 3D foundation models for depth and camera pose [25, 44, 46] provide reliable 3D scene geometry in world coordinates for arbitrary videos. Building on the pre-

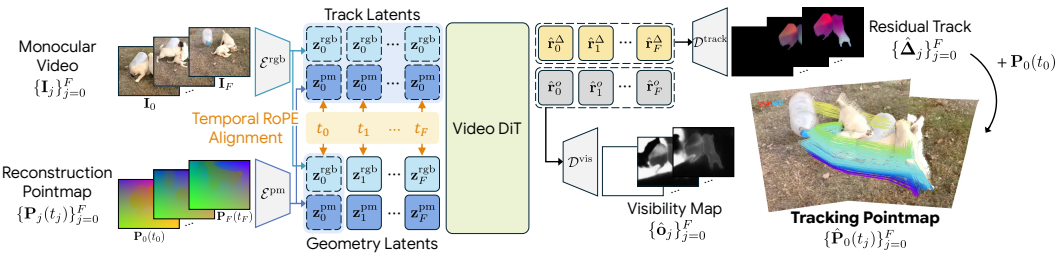

Figure 1: **Overall architecture.** Each RGB frame $\mathbf{I}_j$ and its reconstruction pointmap $\mathbf{P}_j(t_j)$ are encoded into RGB and pointmap latents using separate VAE encoders. A geometry latent is formed by channel-wise concatenation, and a track latent replicates the first-frame geometry latent across all frames. The latents are concatenated along the token dimension and processed by a video DiT, where RoPE assigns the same temporal index to each frame. The track latent outputs are decoded using separate VAE decoders into a residual track $\hat{\mathbf{\Delta}}_j$ and visibility $\hat{\mathbf{o}}_j$.

trained spatio-temporal priors of video diffusion transformers (DiTs), we leverage this 3D geometry as input and repurpose a video DiT to regress dense 3D tracks directly in this coordinate frame.

Specifically, we adopt two pointmap representations [13, 17, 65] that encode 3D geometry and motion: a *frame-anchored* pointmap as input and a *reference-anchored* pointmap as output. In Sec. 4.1, we formulate these pointmaps and define the problem.

However, the frame-anchored generative paradigm of video DiTs is fundamentally misaligned with dense 3D tracking, which requires reference-anchored predictions of the same physical points across time. To address this, we repurpose a video DiT with *dual-latent representation* and *temporal RoPE alignment*. Sec. 4.2 provides further details on the model architecture.

4.1 Problem Formulation

Following [13, 65], given a monocular video $\mathbf{V} = \{\mathbf{I}_t\}_{t=0}^{F} \in \mathbb{R}^{(1+F)\times H\times W\times 3}$, we define a time-dependent pointmap $\mathbf{P}_i(t_j) \in \mathbb{R}^{H\times W\times 3}$ as the 3D positions of the physical content observed in frame $\mathbf{I}_i$ at timestamp t_j. This provides a unified representation of dynamic scenes, jointly encoding 3D geometry and motion. All pointmaps are expressed in a shared world coordinate frame (we use the first frame as the reference frame), and we omit the coordinate index for simplicity.

Reconstruction Pointmap. Each frame $\mathbf{I}_j \in \mathbb{R}^{H\times W\times 3}$ is lifted to 3D using depth and camera intrinsics, and transformed into the shared world coordinate frame via camera extrinsics. This yields a *frame-anchored* reconstruction pointmap $\mathbf{P}_j(t_j) \in \mathbb{R}^{H\times W\times 3}$, which represents the 3D positions of the content in frame $\mathbf{I}_j$ at its own timestamp t_j. Note that such pointmaps can be readily obtained either from ground-truth [16, 32, 86] or from estimated depth and camera pose using recent 3D foundation models [25, 44, 46].

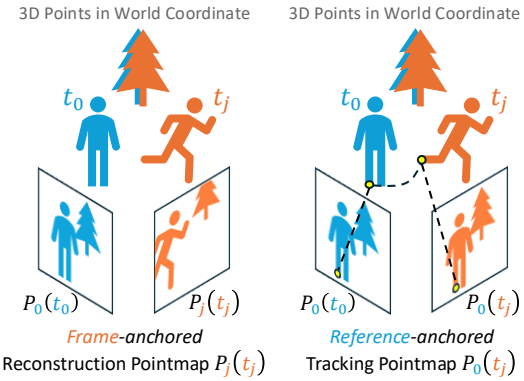

Figure 2: **Pointmap Representations.** Given 3D points of a dynamic scene in world coordinates, the reconstruction pointmap represents 3D points of $\mathbf{I}_j$'s content at t_j, while the tracking pointmap represents 3D points of $\mathbf{I}_0$ (reference frame) at t_j, so that all 3D points of $\mathbf{I}_0$ are tracked across time.

Tracking Pointmap. To enable tracking, we define a *reference-anchored* tracking pointmap $\mathbf{P}_0(t_j) \in \mathbb{R}^{H\times W\times 3}$, which represents the 3D positions of the content originally observed in the reference frame $\mathbf{I}_0$ at timestamp t_j. Here, the reference index is fixed to 0 while time varies, so the same physical points from $\mathbf{I}_0$ are tracked consistently across frames. Fig. 2 illustrates both pointmaps.

Our Objective. Given a video $\mathbf{V} = \{\mathbf{I}_j\}_{j=0}^{F}$ and its reconstruction pointmaps $\{\mathbf{P}_j(t_j)\}_{j=0}^{F}$, which provide per-frame 3D geometry in a shared world coordinate frame, our goal is to predict the tracking pointmaps $\{\mathbf{P}_0(t_j)\}_{j=0}^{F}$ that establish dense 3D correspondences across time by tracking the physical

content of the reference frame $\mathbf{I}_0$ throughout the sequence. In addition, we predict visibility maps $\{\mathbf{o}_j\}_{j=0}^{F}$, where $\mathbf{o}_j \in [0,1]^{H\times W}$ indicates whether each tracked point from $\mathbf{I}_0$ is visible at time t_j.

4.2 Model Architecture

An overview of our architecture is shown in Fig. 1. Given a video $\{\mathbf{I}_j\}_{j=0}^{F}$ and its reconstruction pointmaps $\{\mathbf{P}_j(t_j)\}_{j=0}^{F}$, we encode each RGB frame and pointmap independently using separate VAE encoders $\mathcal{E}^{\text{rgb}}$ and $\mathcal{E}^{\text{pm}}$, yielding per-frame RGB latents $\mathbf{z}_j^{\text{rgb}}$ and pointmap latents $\mathbf{z}_j^{\text{pm}}$:

$$\mathbf{z}_j^{\text{rgb}} = \mathcal{E}^{\text{rgb}}(\mathbf{I}_j) \in \mathbb{R}^{h\times w\times c}, \quad \mathbf{z}_j^{\text{pm}} = \mathcal{E}^{\text{pm}}(\mathbf{P}_j(t_j)) \in \mathbb{R}^{h\times w\times c}. \tag{2}$$

To preserve per-frame spatial precision, we bypass temporal compression in the original 3D VAE by treating the temporal dimension as a batch dimension [53] (see the ablation in Tab. 3).

Point Map Normalization. Prior to VAE encoding, each pointmap is normalized by subtracting the mean and dividing by the maximum distance from the mean, both computed over points whose depths fall within the 2%–98% percentile range across all frames to exclude outliers. As a result, the normalized values lie approximately within $[-1, 1]$.

Dual-Latent Representation. To repurpose a video DiT for reference-anchored 3D tracking, we define two types of latents for the model input: a *geometry latent* $\mathbf{g}_j$, which encodes 3D geometry at timestamp t_j, and a *first-frame-anchored track latent* $\mathbf{r}_j$, which serves as a dense query anchored to the reference frame $\mathbf{I}_0$ for tracking across time.

To explicitly couple RGB appearance $\mathbf{z}_j^{\text{rgb}}$ and 3D geometry $\mathbf{z}_j^{\text{pm}}$ at each spatial location, the geometry latent $\mathbf{g}_j$ is formed by channel-wise concatenation at timestamp t_j. To anchor tracking to the reference frame, the track latent $\mathbf{r}_j$ is obtained by replicating the first-frame geometry latent across all timestamps:

$$\mathbf{g}_j = [\mathbf{z}_j^{\text{rgb}};\ \mathbf{z}_j^{\text{pm}}] \in \mathbb{R}^{h\times w\times 2c}, \qquad \mathbf{r}_j = \mathbf{g}_0 \in \mathbb{R}^{h\times w\times 2c}, \tag{3}$$

where $[\cdot;\cdot]$ denotes channel-wise concatenation.

We concatenate the geometry and track latents along the token dimension and process them with a video DiT f_θ:

$$\{\hat{\mathbf{r}}_j\}_{j=0}^{F} = f_\theta\big([\{\mathbf{g}_j\}_{j=0}^{F},\ \{\mathbf{r}_j\}_{j=0}^{F}]\big), \tag{4}$$

where $[\cdot,\cdot]$ denotes concatenation along the token sequence dimension. The outputs corresponding to the track latents, $\hat{\mathbf{r}}_j \in \mathbb{R}^{h\times w\times 2c}$, are used for tracking pointmap and visibility prediction.

Intuitively, RGB latents provide cues for spatial matching, while pointmap latents store the associated 3D positions. Once $\mathbf{z}_0^{\text{rgb}}(u_r, v_r)$ in the track latent $\mathbf{r}_j$ matches the same physical point as $\mathbf{z}_j^{\text{rgb}}(u_g, v_g)$ in the geometry latent $\mathbf{g}_j$ via attention, the corresponding pointmap latent $\mathbf{z}_j^{\text{pm}}(u_g, v_g)$ directly provides its 3D position $\mathbf{P}_j(t_j)(u_g, v_g)$, which defines the tracked point $\mathbf{P}_0(t_j)(u_r, v_r)$. Here, (u_r, v_r) denotes spatial coordinates in the track latent, and (u_g, v_g) denotes the corresponding spatial coordinates in the geometry latent.

To convert the video DiT into a one-step regressor, we fix the diffusion timestep to zero and use a null text prompt. We further evaluate the inference efficiency of our one-step model in Tab. 6.

Temporal RoPE Alignment. To ensure that each track latent attends to the geometry latent at the correct timestamp, we utilize the temporal axis of 3D RoPE [64]. As illustrated in Fig. 1, we assign both $\mathbf{g}_j$ and $\mathbf{r}_j$ the same temporal RoPE index t_j (Eq. 1). Since RoPE encodes relative position, tokens with identical temporal indices exhibit stronger attention. Consequently, each track latent $\mathbf{r}_j$ attends to the geometry latent $\mathbf{g}_j$ at timestamp t_j, retrieving the corresponding 3D position.

Fig. 3(a) visualizes the query–key attention from $\mathbf{r}_5$ to $\{\mathbf{g}_k\}_{k=0}^{F}$, showing that attention is predominantly localized on $\mathbf{g}_5$, confirming that temporal RoPE alignment correctly specifies the target timestamp. Fig. 3(b) further visualizes the attention between $\mathbf{r}_5$ and $\mathbf{g}_5$ across different transformer layers, showing that full 3D attention effectively establishes accurate correspondences between track and geometry latents under motion. Full attention visualizations and additional discussion are provided in the Appendix E.

Trajectory and Visibility Prediction. We decode the video DiT outputs corresponding to the track latents, $\hat{\mathbf{r}}_j$, into a tracking pointmap $\hat{\mathbf{P}}_0(t_j)$ and a visibility map $\hat{\mathbf{o}}_j$. The latent $\hat{\mathbf{r}}_j \in \mathbb{R}^{h\times w\times 2c}$ is

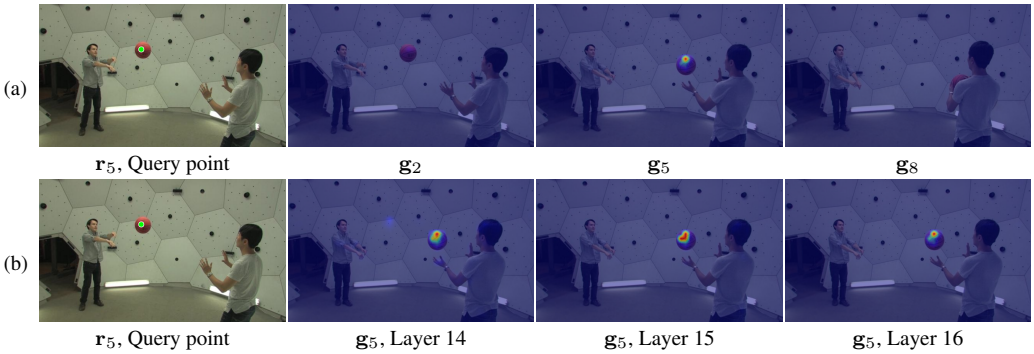

Figure 3: **Query-key attention visualization.** The query point is marked as a green circle. (a) Attention from track latents $\mathbf{r}_5$ at timestamp t_5 to geometry latents $\{\mathbf{g}_j\}_{j=0}^{F}$. Attention is predominantly localized on $\mathbf{g}_5$, showing that RoPE correctly assigns a target timestamp to each track latent. (b) Within $\mathbf{g}_5$, attention aligns with the same physical point under motion, demonstrating accurate dense correspondence between track and geometry latents.

channel-wise partitioned into two components: the first half is used for pointmap prediction, and the second half for visibility prediction.

Instead of directly regressing $\mathbf{P}_0(t_j)$, we predict a residual track with respect to the reference frame:

$$\mathbf{\Delta}_j = \mathbf{P}_0(t_j) - \mathbf{P}_0(t_0). \tag{5}$$

This residual formulation stabilizes training and improves accuracy (see Tab. 3), as $\mathbf{\Delta}_j = \mathbf{0}$ for static regions while non-zero values capture motion-induced displacement.

We decode $\hat{\mathbf{r}}_j$ using two separate VAE decoder heads:

$$\hat{\mathbf{\Delta}}_j = \mathcal{D}^{\text{track}}(\hat{\mathbf{r}}_j^{\Delta}), \qquad \hat{\mathbf{o}}_j = \mathcal{D}^{\text{vis}}(\hat{\mathbf{r}}_j^{o}), \tag{6}$$

where $\hat{\mathbf{r}}_j^{\Delta}$ and $\hat{\mathbf{r}}_j^{o}$ denote the channel-wise partitions. Here, $\hat{\mathbf{\Delta}}_j \in \mathbb{R}^{H\times W\times 3}$ is defined in the normalized pointmap space, and $\hat{\mathbf{o}}_j \in [0,1]^{H\times W}$ denotes visibility.

Since the VAE decoder produces three-channel outputs, the visibility map is broadcast to three channels to match the output dimensionality [36]. For pointmap normalization, we use the same factors (mean and maximum distance) as those of $\mathbf{P}_j(t_j)$ to ensure that the same physical point has the same 3D position after normalization.

Finally, the tracking pointmap is recovered as:

$$\hat{\mathbf{P}}_0(t_j) = \mathbf{P}_0(t_0) + \hat{\mathbf{\Delta}}_j. \tag{7}$$

Long-Video Inference. Our model is trained on clips of $1{+}F$ frames. To handle longer videos at inference time, we adopt a strided sliding window strategy with the first frame as a fixed anchor.

Given a test video of L frames, we compute the stride as $s = \lceil (L{-}1)/F \rceil$ and partition the frames $\{1, \ldots, L{-}1\}$ into s non-overlapping groups. Each forward pass processes the anchor frame $\mathbf{I}_0$ together with F frames sampled from one group, resulting in s passes that cover the entire sequence. For each pass, we assign consecutive RoPE temporal indices $\{0, 1, \ldots, F\}$ as in training, regardless of the original frame indices. As in [13, 20], the model is trained with various temporal strides and naturally generalizes to non-consecutive frames. The predicted pointmaps are consistent across passes without post-processing, as all inputs $\mathbf{P}_j(t_j)$ share a common world coordinate frame. Fig. 5 further evaluates the robustness of our method on long videos and large temporal strides.

5 Experiment

5.1 Implementation Details

Architecture. We fine-tune Wan 2.1-T2V [69] using LoRA [23]. Because the input and output token channel dimensions are doubled, we duplicate the DiT input projection weights [5]. For the output

Table 1: **3D tracking comparison.** We report AJ, APD_{3D}, and OA after Sim(3) alignment. The best and second-best results are highlighted in dark and light blue, respectively.

Method	ADT [56]			PStudio [31]			DR [32]			PO [86]			Kubric [16]			Average		
	AJ↑	APD_{3D}↑	OA↑	AJ↑	APD_{3D}↑	OA↑	AJ↑	APD_{3D}↑	OA↑	AJ↑	APD_{3D}↑	OA↑	AJ↑	APD_{3D}↑	OA↑	AJ↑	APD_{3D}↑	OA↑
(i) Iterative dense 3D trackers																		
DELTA [54] + ViPE [25]	0.5088	0.6949	0.8142	0.4987	0.7810	0.6959	0.4049	0.5847	0.7638	0.4559	0.6286	0.8116	0.2894	0.3721	0.9630	0.4315	0.6123	0.8097
DELTAv2 [55] + ViPE [25]	0.5135	0.7066	0.8038	0.5353	0.8026	0.7284	0.4167	0.5888	0.7825	0.4459	0.6246	0.8011	0.2860	0.3692	0.9564	0.4395	0.6184	0.8144
DELTAv2 [55] + DA3 [46]	0.6150	0.8219	0.8125	0.5571	0.8496	0.7087	0.4494	0.6217	0.7817	0.5304	0.7251	0.8020	0.3354	0.4106	0.9592	0.4975	0.6858	0.8128
(ii) Feed-forward dense 3D trackers based on 3D reconstruction models																		
St4RTrack [13]	0.5929	0.7683	0.8323	0.5723	0.7552	0.8099	0.3534	0.5710	0.6836	0.3968	0.6579	0.6860	0.1193	0.1896	0.7703	0.4069	0.5884	0.7564
Any4D [35]	0.4646	0.6134	0.8358	0.4222	0.5707	0.8128	0.4414	0.6955	0.6801	0.4387	0.6830	0.7353	0.3887	0.4967	0.8826	0.4311	0.6119	0.7893
TraceAnything [49]	0.5929	0.7634	0.8412	0.5225	0.6928	0.8130	0.2072	0.3549	0.7332	0.2041	0.3649	0.6930	0.2418	0.3252	0.8198	0.3537	0.5002	0.7800
(iii) Feed-forward dense 3D trackers based on video generative models																		
MotionCrafter [87]	0.4460	0.6037	0.8036	0.5044	0.6659	0.8142	0.4926	0.6172	0.9172	0.4197	0.6412	0.7301	0.2176	0.3011	0.8730	0.4161	0.5658	0.8276
TrackCraft3R + ViPE [25]	0.6683	0.7688	0.9405	0.6803	0.8163	0.8937	0.5842	0.7034	0.9408	0.5836	0.7262	0.8943	0.3032	0.3940	0.9597	0.5639	0.6817	0.9258
TrackCraft3R + DA3 [46]	0.8626	0.9510	0.9445	0.7287	0.8713	0.8891	0.6518	0.7706	0.9388	0.7288	0.8678	0.8938	0.4208	0.5047	0.9587	0.6785	0.7931	0.9250

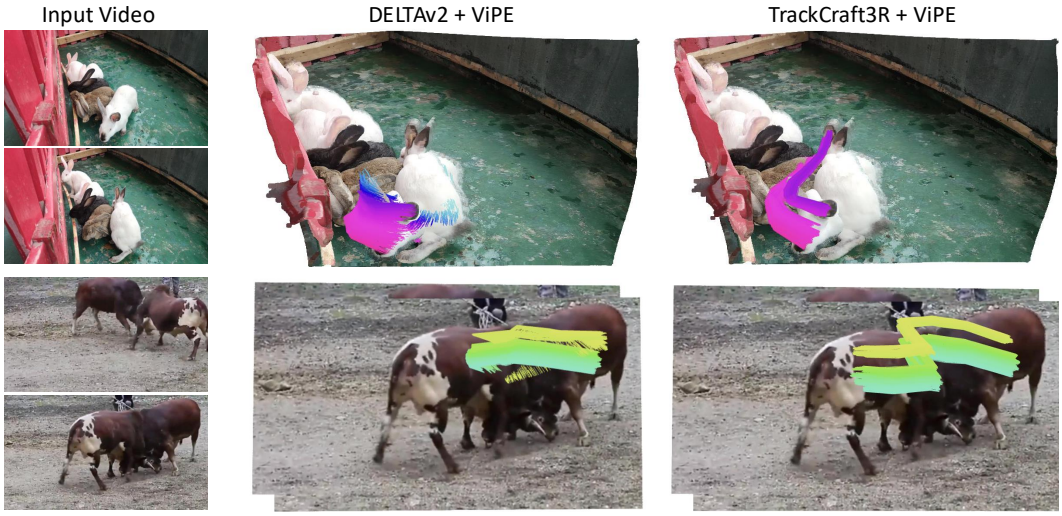

Figure 4: **Qualitative comparison on ITTO [10] videos.** TrackCraft3R accurately estimates dense 3D trajectories on real-world videos under large object dynamics and occlusion.

projection, we retain the pre-trained weights for the first half of the channels and zero-initialize the remaining half. All VAE components are initialized from the pre-trained Wan VAE weights.

Training. All models are trained at a resolution of 480×832 on 12-frame clips using 8 H200 GPUs. Training proceeds in two stages. In Stage 1, we train the DiT with LoRA and input/output projection layers, with VAEs being frozen. We use AdamW [50] with a learning rate of 1e-4 and a global batch size of 80 for 3 days. In Stage 2, we unfreeze all VAE encoders and decoders, $\mathcal{E}^{\text{rgb}}, \mathcal{E}^{\text{pm}}, \mathcal{D}^{\text{track}}, \mathcal{D}^{\text{vis}}$, and continue end-to-end training with learning rates of 3e-5 for the DiT and 1e-5 for the VAE, using a global batch size of 64 for an additional 2 days.

Training Objective. We minimize an MSE loss [55] on the predicted residual $\hat{\mathbf{\Delta}}_j$ in normalized pointmap space, combined with a BCE loss [34] on visibility $\hat{\mathbf{o}}_j$, weighted by 0.1.

Dataset. Following [13], we train our model on Kubric [16], PointOdyssey [86], and Dynamic Replica [32], which provide ground-truth 3D trajectories from mesh vertices. We also include TartanAir [73], a static-scene dataset with large camera motion, to improve robustness to ego-motion. More details are provided in Appendix A.

5.2 Evaluation Settings

Evaluation Datasets. We evaluate our method on both 3D sparse and dense tracking benchmarks, with all metrics computed in a world coordinate frame. For *3D sparse tracking*, following [13], we use two real-world datasets from TAPVid-3D [41], Aerial Digital Twin (ADT) [56] and Panoptic Studio (PStudio) [31], along with two synthetic test dataset, Point Odyssey (PO) [86] and Dynamic Replica (DR) [32]. Each dataset provides sparse ground-truth 3D trajectories, and we evaluate the first 84 frames. For *3D dense tracking*, following [35, 54, 55], we use the held-out Kubric [16] test

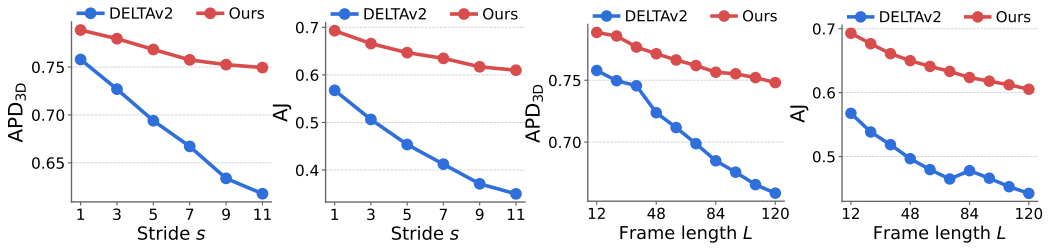

(a) APD_{3D}, varying s (b) AJ, varying s (c) APD_{3D}, varying L (d) AJ, varying L

Figure 5: **Robustness to large inter-frame motion (a, b) and long videos (c, d). TrackCraft3R**'s performance drops much more slowly than **DELTAv2** as stride s or frame length L grows.

split consisting of 50 sequences. This dataset provides dense ground-truth 3D trajectories defined for every pixel in the reference frame, and we evaluate the first 24 frames following [55].

Evaluation Metrics. Following TAPVid-3D [41], we report three metrics: (i) *average percentage of points within* δ_{3D} (APD_{3D}), defined as the percentage of points whose 3D end-point error is below a threshold $\delta_{3D} \in \{0.1, 0.3, 0.5, 1\}$m [13], averaged over thresholds; (ii) *occlusion accuracy* (OA), which measures the accuracy of occlusion prediction as a binary classification task; and (iii) *average Jaccard* (AJ), which jointly measures 3D point accuracy and occlusion prediction. Predicted trajectories are aligned to the ground truth using Sim(3) alignment [13, 76].

Baselines. We compare our method against recent dense 3D trackers, grouped into three categories. *(i) Iterative Dense 3D Trackers*: DELTA [54] and DELTAv2 [55], which condition on external depth and use camera poses to transform tracks into world coordinates. *(ii) Feed-forward Dense 3D Trackers Based on 3D Reconstruction Models*: St4RTrack [13], Any4D [35], and TraceAnything [49] are built upon pre-trained 3D reconstruction backbones [37, 42, 79], which are pre-trained to predict camera poses, depth, or pointmaps. *(iii) Feed-forward Dense 3D Trackers Based on Video Generative Models*: MotionCrafter [87], based on a video diffusion U-Net [3], where tracks are obtained by chaining scene flow across adjacent frames. Since *(ii)* does not output visibility, we project the predicted track pointmaps into each frame and consider a point visible if the projected pixel lies within the image bounds and its projected depth is within a 10% tolerance of the per-frame depth. We use ViPE [25] and DA3 [46] to provide input geometry for DELTA, DELTAv2, and TrackCraft3R.

Quantitative Comparison. In Tab. 1, TrackCraft3R achieves state-of-the-art performance across all benchmarks, with the best average AJ, APD_{3D}, and OA. TrackCraft3R + ViPE surpasses the strongest iterative dense 3D tracker, DELTAv2 [55] + ViPE, as well as all feed-forward baselines. TrackCraft3R + ViPE is even competitive with DELTAv2 [55] + DA3. With the stronger 3D foundation model DA3, TrackCraft3R + DA3 further surpasses DELTAv2 + DA3 and outperforms all other feed-forward baselines by a large margin. More quantitative comparisons with a dense 2D tracker [20], sparse 3D trackers [76, 84], and the concurrent work V-DPM [65] are provided in Appendix Secs. B, C, and D.

Qualitative Comparison. Fig. 4 compares 3D trajectories predicted by TrackCraft3R and DELTAv2 [55] on real-world ITTO [10] videos. TrackCraft3R produces accurate dense trajectories under large object dynamics and occlusion, where DELTAv2 often fails. Additional results on ITTO [10] and DAVIS [57] are provided in Appendix Sec. F and the supplementary video.

Robustness to Large Motion and Long Videos. We further evaluate the robustness of our method with respect to *motion* and *video length*. For *large motion*, we fix the clip length to 12 frames and increase the temporal stride s from 1 to 12 (in steps of 1), enlarging per-frame displacement. For *long videos*, we fix the stride to s=1 and increase the sequence length L from 12 to 120 (in steps of 12). The resulting APD_{3D} and AJ curves are shown in Fig. 5, averaged over sparse tracking benchmarks. TrackCraft3R consistently widens the gap with DELTAv2 [55] in both settings, indicating that the learned motion prior enables robust tracking under large displacements and generalizes to long-horizon videos beyond the training sequence length (12 frames).

5.3 Ablation Study

All ablation studies report the average AJ, APD_{3D}, and OA across all benchmarks, and use ViPE [25] for input geometry, unless otherwise specified.

Table 2: **Ablation on spatio-temporal priors.**

Initialization	AJ↑	APD_{3D}↑	OA↑
Random	0.4698	0.6312	0.8271
Pre-trained (Ours)	**0.5639**	**0.6817**	**0.9258**

Spatio-Temporal Prior in Video DiT. We compare our model against an identical architecture trained from scratch, both to convergence on the same data. Tab. 2 shows that random initialization substantially degrades all metrics, confirming that the pre-trained spatio-temporal prior is critical.

Model Design. Tab. 3 ablates four core design components by removing each from the full model. For this ablation, we train each model with the VAE frozen. *(a) w/o First-frame anchoring*: setting $\mathbf{r}_j = \mathbf{g}_j$ instead of $\mathbf{r}_j = \mathbf{g}_0$, removing reference-frame anchoring. *(b) w/o Temporal RoPE alignment*: assigning a constant temporal index t_0 to all $\mathbf{r}_j$. *(c) w/o Residual displacement*: directly regressing the 3D track pointmap $\mathbf{P}_0(t_j)$ instead of predicting residual displacements $\mathbf{\Delta}_j$. *(d) w/ VAE temporal compression*: using the original 3D VAE temporal downsampling instead of processing frames independently. All four components contribute. (a) causes consistent drops across all metrics and (b) causes the largest AJ drop, indicating that (a) and (b) jointly contribute to reference-anchored correspondence at the correct target timestamp (Fig. 3). (c) specifically drops APD_{3D}, since residual prediction stabilizes pointmap prediction. (d) drops all metrics consistently, as VAE temporal compression affects both the pointmap and visibility decoders.

Table 3: **Ablation on model components.**

Configuration	AJ↑	APD_{3D}↑	OA↑
(a) w/o First-frame anchoring	0.5135	0.6535	0.8778
(b) w/o Temporal RoPE alignment	0.4450	0.6317	0.8031
(c) w/o Residual displacement	0.5007	0.6172	0.9159
(d) w/ VAE temporal compression	0.4487	0.6325	0.8148
Full model (Ours)	**0.5609**	**0.6790**	**0.9225**

Input Geometry Quality. In Tab. 4, we study the impact of input geometry quality by using depth and camera poses from DA3 [46] and ground truth (GT). Metrics are averaged over the synthetic datasets [16, 32, 86], for which GT is available. Without any retraining, replacing DA3 with GT consistently improves all metrics, providing an upper bound for our method and suggesting that future advances in 3D geometry estimation can directly translate to better tracking performance. Note that performing tracking with input geometry from off-the-shelf estimators is becoming a common practice [54, 55, 76, 84]. In Appendix Sec. C, we further compare TrackCraft3R with recent sparse 3D trackers [76, 84] under the same input geometry.

Table 4: **Ablation on input geometry.**

Configuration	AJ↑	APD_{3D}↑	OA↑
DELTAv2 [55] + DA3 [46]	0.4384	0.5858	0.8476
TrackCraft3R + DA3 [46]	**0.6005**	**0.7144**	**0.9304**
DELTAv2 [55] + GT	0.5590	0.7169	0.8380
TrackCraft3R + GT	**0.7649**	**0.8635**	**0.9353**

LoRA Rank and VAE Finetuning. In Tab. 5, increasing the LoRA rank from 64 to 1024 consistently improves performance, indicating that the DiT benefits from more expressive low-rank updates. Unfreezing the VAEs in Stage 2 yields further gains, confirming the benefit of adapting them to the pointmap and visibility domains.

Table 5: **Ablation on LoRA rank and VAE finetuning.**

LoRA rank	VAE finetuning	AJ↑	APD_{3D}↑	OA↑
64	✗	0.5025	0.6430	0.8779
256	✗	0.5399	0.6623	0.9112
1024	✗	0.5609	0.6790	0.9225
1024	✓	**0.5639**	**0.6817**	**0.9258**

Inference Efficiency. Tab. 6 compares inference time and peak GPU memory of TrackCraft3R, DELTA [54], and DELTAv2 [55] at 448×448 resolution for 12- and 23-frame clips on a single NVIDIA A6000 GPU. For 12 frames, TrackCraft3R is **1.3× faster** and uses **4.6× less peak memory** than DELTAv2. Specifically, DELTA and DELTAv2 (1) perform iterative refinement (six steps) and (2) construct 4D correlation features between dense queries and multi-scale image features. In contrast, TrackCraft3R (1) predicts trajectories in a *single forward pass* and (2) replaces explicit 4D correlation features with full 3D attention in a $1/16$ *spatially compressed latent space*, which is effectively upsampled to pixel space with a VAE decoder. For longer sequences (*e.g.*, 23 frames), the same trend holds: all methods scale roughly linearly in runtime, while peak memory remains similar.

Table 6: **Inference efficiency** with different frame lengths.

Frames	Method	Time (s)↓	Memory (GB)↓
12	DELTA [54]	14.64	29.97
12	DELTAv2 [55]	5.00	35.46
12	**TrackCraft3R**	**3.91**	**7.63**
23	DELTA [54]	28.92	30.78
23	DELTAv2 [55]	9.70	35.90
23	**TrackCraft3R**	**7.84**	**7.63**

6 Conclusion

We presented TrackCraft3R, the first method to repurpose a video diffusion transformer as a single-pass dense 3D tracker. By introducing a dual-latent representation that couples per-frame geometry latents with first-frame-anchored track latents, together with a temporal RoPE alignment that specifies the target timestamp of each track latent, TrackCraft3R converts the per-frame generative paradigm of video DiTs into a reference-anchored dense tracking paradigm with LoRA fine-tuning. TrackCraft3R achieves state-of-the-art performance on standard 3D sparse and dense tracking benchmarks while running $1.3\times$ faster and using $4.6\times$ less peak memory than the strongest iterative 3D tracker, and further demonstrates robustness to large motions and long videos.

References

[1] Manuel López Antequera, Pau Gargallo, Markus Hofinger, Samuel Rota Bulo, Yubin Kuang, and Peter Kontschieder. Mapillary planet-scale depth dataset. In *European Conference on Computer Vision*, pages 589–604. Springer, 2020.

[2] Homanga Bharadhwaj, Roozbeh Mottaghi, Abhinav Gupta, and Shubham Tulsiani. Track2Act: Predicting point tracks from internet videos enables generalizable robot manipulation. In *European Conference on Computer Vision*, pages 306–324. Springer, 2024.

[3] Andreas Blattmann, Tim Dockhorn, Sumith Kulal, Daniel Mendelevitch, Maciej Kilian, Dominik Lorenz, Yam Levi, Zion English, Vikram Voleti, Adam Letts, et al. Stable video diffusion: Scaling latent video diffusion models to large datasets. *arXiv preprint arXiv:2311.15127*, 2023.

[4] Yohann Cabon, Naila Murray, and Martin Humenberger. Virtual KITTI 2. *arXiv preprint arXiv:2001.10773*, 2020.

[5] Hila Chefer, Uriel Singer, Amit Zohar, Yuval Kirstain, Adam Polyak, Yaniv Taigman, Lior Wolf, and Shelly Sheynin. VideoJam: Joint appearance-motion representations for enhanced motion generation in video models. *arXiv preprint arXiv:2502.02492*, 2025.

[6] Seokju Cho, Jiahui Huang, Jisu Nam, Honggyu An, Seungryong Kim, and Joon-Young Lee. Local all-pair correspondence for point tracking. In *European conference on computer vision*, pages 306–325. Springer, 2024.

[7] Seokju Cho, Jiahui Huang, Seungryong Kim, and Joon-Young Lee. Seurat: From moving points to depth. In *Proceedings of the Computer Vision and Pattern Recognition Conference*, pages 7211–7221, 2025.

[8] Angela Dai, Angel X Chang, Manolis Savva, Maciej Halber, Thomas Funkhouser, and Matthias Nießner. ScanNet: Richly-annotated 3D reconstructions of indoor scenes. In *Proceedings of the IEEE conference on computer vision and pattern recognition*, pages 5828–5839, 2017.

[9] Matt Deitke, Dustin Schwenk, Jordi Salvador, Luca Weihs, Oscar Michel, Eli VanderBilt, Ludwig Schmidt, Kiana Ehsani, Aniruddha Kembhavi, and Ali Farhadi. Objaverse: A universe of annotated 3D objects. In *Proceedings of the IEEE/CVF conference on computer vision and pattern recognition*, pages 13142–13153, 2023.

[10] Ilona Demler, Saumya Chauhan, and Georgia Gkioxari. Is this tracker on? a benchmark protocol for dynamic tracking. *arXiv preprint arXiv:2510.19819*, 2025.

[11] Carl Doersch, Ankush Gupta, Larisa Markeeva, Adria Recasens, Lucas Smaira, Yusuf Aytar, Joao Carreira, Andrew Zisserman, and Yi Yang. Tap-Vid: A benchmark for tracking any point in a video. *Advances in Neural Information Processing Systems*, 35:13610–13626, 2022.

[12] Carl Doersch, Yi Yang, Mel Vecerik, Dilara Gokay, Ankush Gupta, Yusuf Aytar, Joao Carreira, and Andrew Zisserman. TAPIR: Tracking any point with per-frame initialization and temporal refinement. In *Proceedings of the IEEE/CVF International Conference on Computer Vision*, pages 10061–10072, 2023.

[13] Haiwen Feng, Junyi Zhang, Qianqian Wang, Yufei Ye, Pengcheng Yu, Michael J. Black, Trevor Darrell, and Angjoo Kanazawa. St4RTrack: Simultaneous 4D reconstruction and tracking in the world. In *Proceedings of the IEEE/CVF International Conference on Computer Vision*, pages 8503–8513, 2025.

[14] Xiao Fu, Wei Yin, Mu Hu, Kaixuan Wang, Yuexin Ma, Ping Tan, Shaojie Shen, Dahua Lin, and Xiaoxiao Long. GeoWizard: Unleashing the diffusion priors for 3D geometry estimation from a single image. In *European Conference on Computer Vision*, pages 241–258. Springer, 2024.

[15] Daniel Geng, Charles Herrmann, Junhwa Hur, Forrester Cole, Serena Zhang, Tobias Pfaff, Tatiana Lopez-Guevara, Yusuf Aytar, Michael Rubinstein, Chen Sun, et al. Motion prompting: Controlling video generation with motion trajectories. In *Proceedings of the Computer Vision and Pattern Recognition Conference*, pages 1–12, 2025.

[16] Klaus Greff, Francois Belletti, Lucas Beyer, Carl Doersch, Yilun Du, Daniel Duckworth, David J. Fleet, Dan Gnanapragasam, Florian Golemo, Charles Herrmann, et al. Kubric: A scalable dataset generator. In *Proceedings of the IEEE/CVF conference on computer vision and pattern recognition*, pages 3749–3761, 2022.

[17] Jisang Han, Honggyu An, Jaewoo Jung, Takuya Narihira, Junyoung Seo, Kazumi Fukuda, Chaehyun Kim, Sunghwan Hong, Yuki Mitsufuji, and Seungryong Kim. D^2USt3R: Enhancing 3D reconstruction for dynamic scenes. *arXiv preprint arXiv:2504.06264*, 2025.

[18] Jisang Han, Sunghwan Hong, Jaewoo Jung, Wooseok Jang, Honggyu An, Qianqian Wang, Seungryong Kim, and Chen Feng. Emergent outlier view rejection in visual geometry grounded transformers. *arXiv preprint arXiv:2512.04012*, 2025.

[19] Adam W. Harley, Zhaoyuan Fang, and Katerina Fragkiadaki. Particle video revisited: Tracking through occlusions using point trajectories. In *European Conference on Computer Vision*, pages 59–75. Springer, 2022.

[20] Adam W. Harley, Yang You, Xinglong Sun, Yang Zheng, Nikhil Raghuraman, Yunqi Gu, Sheldon Liang, Wen-Hsuan Chu, Achal Dave, Suya You, et al. AllTracker: Efficient dense point tracking at high resolution. In *Proceedings of the IEEE/CVF International Conference on Computer Vision*, pages 5253–5262, 2025.

[21] Jing He, Haodong Li, Wei Yin, Yixun Liang, Leheng Li, Kaiqiang Zhou, Hongbo Zhang, Bingbing Liu, and Ying-Cong Chen. Lotus: Diffusion-based visual foundation model for high-quality dense prediction. *arXiv preprint arXiv:2409.18124*, 2024.

[22] Eric Hedlin, Gopal Sharma, Shweta Mahajan, Hossam Isack, Abhishek Kar, Andrea Tagliasacchi, and Kwang Moo Yi. Unsupervised semantic correspondence using stable diffusion. *Advances in Neural Information Processing Systems*, 36:8266–8279, 2023.

[23] Edward J. Hu, yelong shen, Phillip Wallis, Zeyuan Allen-Zhu, Yuanzhi Li, Shean Wang, Lu Wang, and Weizhu Chen. LoRA: Low-rank adaptation of large language models. In *International Conference on Learning Representations*, 2022.

[24] Wenbo Hu, Xiangjun Gao, Xiaoyu Li, Sijie Zhao, Xiaodong Cun, Yong Zhang, Long Quan, and Ying Shan. DepthCrafter: Generating consistent long depth sequences for open-world videos. In *Proceedings of the IEEE/CVF Conference on Computer Vision and Pattern Recognition*, pages 2005–2015, 2025.

[25] Jiahui Huang, Qunjie Zhou, Hesam Rabeti, Aleksandr Korovko, Huan Ling, Xuanchi Ren, Tianchang Shen, Jun Gao, Dmitry Slepichev, Chen-Hsuan Lin, et al. ViPE: Video pose engine for 3D geometric perception. *arXiv preprint arXiv:2508.10934*, 2025.

[26] Po-Han Huang, Kevin Matzen, Johannes Kopf, Narendra Ahuja, and Jia-Bin Huang. DeepMVS: Learning multi-view stereopsis. In *Proceedings of the IEEE conference on computer vision and pattern recognition*, pages 2821–2830, 2018.

[27] Wenlong Huang, Yu-Wei Chao, Arsalan Mousavian, Ming-Yu Liu, Dieter Fox, Kaichun Mo, and Li Fei-Fei. PointWorld: Scaling 3D world models for in-the-wild robotic manipulation. *arXiv preprint arXiv:2601.03782*, 2026.

[28] Wonbong Jang, Shikun Liu, Soubhik Sanyal, Juan Camilo Perez, Kam Woh Ng, Sanskar Agrawal, Juan-Manuel Perez-Rua, Yiannis Douratsos, and Tao Xiang. Rays as pixels: Learning a joint distribution of videos and camera trajectories. *arXiv preprint arXiv:2604.09429*, 2026.

[29] Zeren Jiang, Chuanxia Zheng, Iro Laina, Diane Larlus, and Andrea Vedaldi. Geo4D: Leveraging video generators for geometric 4D scene reconstruction. In *Proceedings of the IEEE/CVF International Conference on Computer Vision*, pages 20658–20671, 2025.

[30] Linyi Jin, Richard Tucker, Zhengqi Li, David Fouhey, Noah Snavely, and Aleksander Holynski. Stereo4D: Learning how things move in 3D from internet stereo videos. *arXiv preprint arXiv:2412.09621*, 2024.

[31] Hanbyul Joo, Hao Liu, Lei Tan, Lin Gui, Bart Nabbe, Iain Matthews, Takeo Kanade, Shohei Nobuhara, and Yaser Sheikh. Panoptic studio: A massively multiview system for social motion capture. In *Proceedings of the IEEE international conference on computer vision*, pages 3334–3342, 2015.

[32] Nikita Karaev, Ignacio Rocco, Benjamin Graham, Natalia Neverova, Andrea Vedaldi, and Christian Rupprecht. DynamicStereo: Consistent dynamic depth from stereo videos. In *Proceedings of the IEEE/CVF Conference on Computer Vision and Pattern Recognition*, pages 13229–13239, 2023.

[33] Nikita Karaev, Ignacio Rocco, Benjamin Graham, Natalia Neverova, Andrea Vedaldi, and Christian Rupprecht. CoTracker: It is better to track together. In *European conference on computer vision*, pages 18–35. Springer, 2024.

[34] Nikita Karaev, Yuri Makarov, Jianyuan Wang, Natalia Neverova, Andrea Vedaldi, and Christian Rupprecht. CoTracker3: Simpler and better point tracking by pseudo-labelling real videos. In *Proceedings of the IEEE/CVF International Conference on Computer Vision*, pages 6013–6022, 2025.

[35] Jay Karhade, Nikhil Keetha, Yuchen Zhang, Tanisha Gupta, Akash Sharma, Sebastian Scherer, and Deva Ramanan. Any4D: Unified feed-forward metric 4D reconstruction. *arXiv preprint arXiv:2512.10935*, 2025.

[36] Bingxin Ke, Anton Obukhov, Shengyu Huang, Nando Metzger, Rodrigo Caye Daudt, and Konrad Schindler. Repurposing diffusion-based image generators for monocular depth estimation. In *Proceedings of the IEEE/CVF conference on computer vision and pattern recognition*, pages 9492–9502, 2024.

[37] Nikhil Keetha, Norman Müller, Johannes Schönberger, Lorenzo Porzi, Yuchen Zhang, Tobias Fischer, Arno Knapitsch, Duncan Zauss, Ethan Weber, Nelson Antunes, et al. MapAnything: Universal feed-forward metric 3D reconstruction. *arXiv preprint arXiv:2509.13414*, 2025.

[38] Jisoo Kim, Jungbin Cho, Sanghyeok Chu, Ananya Bal, Jinhyung Kim, Gunhee Lee, Sihaeng Lee, Seung Hwan Kim, Bohyung Han, Hyunmin Lee, et al. Pri4R: Learning world dynamics for vision-language-action models with privileged 4D representation. *arXiv preprint arXiv:2603.01549*, 2026.

[39] Po-Chen Ko, Jiayuan Mao, Yilun Du, Shao-Hua Sun, and Joshua B. Tenenbaum. Learning to act from actionless videos through dense correspondences. *arXiv preprint arXiv:2310.08576*, 2023.

[40] Weijie Kong, Qi Tian, Zijian Zhang, Rox Min, Zuozhuo Dai, Jin Zhou, Jiangfeng Xiong, Xin Li, Bo Wu, Jianwei Zhang, et al. HunyuanVideo: A systematic framework for large video generative models. *arXiv preprint arXiv:2412.03603*, 2024.

[41] Skanda Koppula, Ignacio Rocco, Yi Yang, Joe Heyward, Joao Carreira, Andrew Zisserman, Gabriel Brostow, and Carl Doersch. TapVid-3D: A benchmark for tracking any point in 3D. *Advances in Neural Information Processing Systems*, 37:82149–82165, 2024.

[42] Vincent Leroy, Yohann Cabon, and Jérôme Revaud. Grounding image matching in 3D with MASt3R. In *European conference on computer vision*, pages 71–91. Springer, 2024.

[43] Zhengqi Li and Noah Snavely. MegaDepth: Learning single-view depth prediction from internet photos. In *Proceedings of the IEEE conference on computer vision and pattern recognition*, pages 2041–2050, 2018.

[44] Zhengqi Li, Richard Tucker, Forrester Cole, Qianqian Wang, Linyi Jin, Vickie Ye, Angjoo Kanazawa, Aleksander Holynski, and Noah Snavely. MegaSaM: Accurate, fast and robust structure and motion from casual dynamic videos. In *Proceedings of the IEEE/CVF Conference on Computer Vision and Pattern Recognition*, pages 10486–10496, 2025.

[45] Yiqing Liang, Abhishek Badki, Hang Su, James Tompkin, and Orazio Gallo. Zero-shot monocular scene flow estimation in the wild. In *Proceedings of the Computer Vision and Pattern Recognition Conference*, pages 21031–21044, 2025.

[46] Haotong Lin, Sili Chen, Junhao Liew, Donny Y Chen, Zhenyu Li, Guang Shi, Jiashi Feng, and Bingyi Kang. Depth Anything 3: Recovering the visual space from any views. *arXiv preprint arXiv:2511.10647*, 2025.

[47] Lu Ling, Yichen Sheng, Zhi Tu, Wentian Zhao, Cheng Xin, Kun Wan, Lantao Yu, Qianyu Guo, Zixun Yu, Yawen Lu, et al. DL3DV-10K: A large-scale scene dataset for deep learning-based 3D vision. In *Proceedings of the IEEE/CVF Conference on Computer Vision and Pattern Recognition*, pages 22160–22169, 2024.

[48] Yaron Lipman, Ricky TQ Chen, Heli Ben-Hamu, Maximilian Nickel, and Matt Le. Flow matching for generative modeling. *arXiv preprint arXiv:2210.02747*, 2022.

[49] Xinhang Liu, Yuxi Xiao, Donny Y Chen, Jiashi Feng, Yu-Wing Tai, Chi-Keung Tang, and Bingyi Kang. Trace Anything: Representing any video in 4D via trajectory fields. *arXiv preprint arXiv:2510.13802*, 2025.

[50] Ilya Loshchilov and Frank Hutter. Decoupled weight decay regularization. *arXiv preprint arXiv:1711.05101*, 2017.

[51] Jinjie Mai, Wenxuan Zhu, Haozhe Liu, Bing Li, Cheng Zheng, Jürgen Schmidhuber, and Bernard Ghanem. Can video diffusion model reconstruct 4D geometry? *arXiv preprint arXiv:2503.21082*, 2025.

[52] Jisu Nam, Gyuseong Lee, Sunwoo Kim, Hyeonsu Kim, Hyoungwon Cho, Seyeon Kim, and Seungryong Kim. Diffusion model for dense matching. *arXiv preprint arXiv:2305.19094*, 2023.

[53] Jisu Nam, Soowon Son, Dahyun Chung, Jiyoung Kim, Siyoon Jin, Junhwa Hur, and Seungryong Kim. Emergent temporal correspondences from video diffusion transformers. *arXiv preprint arXiv:2506.17220*, 2025.

[54] Tuan Duc Ngo, Peiye Zhuang, Chuang Gan, Evangelos Kalogerakis, Sergey Tulyakov, Hsin-Ying Lee, and Chaoyang Wang. DELTA: Dense efficient long-range 3D tracking for any video. *arXiv preprint arXiv:2410.24211*, 2024.

[55] Tuan Duc Ngo, Ashkan Mirzaei, Guocheng Qian, Hanwen Liang, Chuang Gan, Evangelos Kalogerakis, Peter Wonka, and Chaoyang Wang. DELTAv2: Accelerating dense 3D tracking. *arXiv preprint arXiv:2508.01170*, 2025.

[56] Xiaqing Pan, Nicholas Charron, Yongqian Yang, Scott Peters, Thomas Whelan, Chen Kong, Omkar Parkhi, Richard Newcombe, and Yuheng Carl Ren. Aria Digital Twin: A new benchmark dataset for egocentric 3D machine perception. In *Proceedings of the IEEE/CVF International Conference on Computer Vision*, pages 20133–20143, 2023.

[57] Jordi Pont-Tuset, Federico Perazzi, Sergi Caelles, Pablo Arbeláez, Alex Sorkine-Hornung, and Luc Van Gool. The 2017 DAVIS challenge on video object segmentation. *arXiv preprint arXiv:1704.00675*, 2017.

[58] Jeremy Reizenstein, Roman Shapovalov, Philipp Henzler, Luca Sbordone, Patrick Labatut, and David Novotny. Common objects in 3D: Large-scale learning and evaluation of real-life 3D category reconstruction. In *Proceedings of the IEEE/CVF international conference on computer vision*, pages 10901–10911, 2021.

[59] Mike Roberts, Jason Ramapuram, Anurag Ranjan, Atulit Kumar, Miguel Angel Bautista, Nathan Paczan, Russ Webb, and Joshua M. Susskind. Hypersim: A photorealistic synthetic dataset for holistic indoor scene understanding. In *Proceedings of the IEEE/CVF international conference on computer vision*, pages 10912–10922, 2021.

[60] Peter Sand and Seth Teller. Particle video: Long-range motion estimation using point trajectories. *International journal of computer vision*, 80(1):72–91, 2008.

[61] Saurabh Saxena, Charles Herrmann, Junhwa Hur, Abhishek Kar, Mohammad Norouzi, Deqing Sun, and David J. Fleet. The surprising effectiveness of diffusion models for optical flow and monocular depth estimation. *Advances in Neural Information Processing Systems*, 36:39443–39469, 2023.

[62] Jiahao Shao, Yuanbo Yang, Hongyu Zhou, Youmin Zhang, Yujun Shen, Vitor Guizilini, Yue Wang, Matteo Poggi, and Yiyi Liao. Learning temporally consistent video depth from video diffusion priors. In *Proceedings of the Computer Vision and Pattern Recognition Conference*, pages 22841–22852, 2025.

[63] Soowon Son, Honggyu An, Chaehyun Kim, Hyunah Ko, Jisu Nam, Dahyun Chung, Siyoon Jin, Jung Yi, Jaewon Min, Junhwa Hur, et al. Repurposing video diffusion transformers for robust point tracking. *arXiv preprint arXiv:2512.20606*, 2025.

[64] Jianlin Su, Murtadha Ahmed, Yu Lu, Shengfeng Pan, Wen Bo, and Yunfeng Liu. RoFormer: Enhanced transformer with rotary position embedding. *Neurocomputing*, 568:127063, 2024.

[65] Edgar Sucar, Eldar Insafutdinov, Zihang Lai, and Andrea Vedaldi. V-DPM: 4D video reconstruction with dynamic point maps. *arXiv preprint arXiv:2601.09499*, 2026.

[66] Pei Sun, Henrik Kretzschmar, Xerxes Dotiwalla, Aurelien Chouard, Vijaysai Patnaik, Paul Tsui, James Guo, Yin Zhou, Yuning Chai, Benjamin Caine, et al. Scalability in perception for autonomous driving: Waymo open dataset. In *Proceedings of the IEEE/CVF conference on computer vision and pattern recognition*, pages 2446–2454, 2020.

[67] Andrew Szot, Alexander Clegg, Eric Undersander, Erik Wijmans, Yili Zhao, John Turner, Noah Maestre, Mustafa Mukadam, Devendra Singh Chaplot, Oleksandr Maksymets, et al. Habitat 2.0: Training home assistants to rearrange their habitat. *Advances in neural information processing systems*, 34:251–266, 2021.

[68] Luming Tang, Menglin Jia, Qianqian Wang, Cheng Perng Phoo, and Bharath Hariharan. Emergent correspondence from image diffusion. *Advances in neural information processing systems*, 36:1363–1389, 2023.

[69] Team Wan, Ang Wang, Baole Ai, Bin Wen, Chaojie Mao, Chen-Wei Xie, Di Chen, Feiwu Yu, Haiming Zhao, Jianxiao Yang, et al. Wan: Open and advanced large-scale video generative models. *arXiv preprint arXiv:2503.20314*, 2025.

[70] Bo Wang, Jian Li, Yang Yu, Li Liu, Zhenping Sun, and Dewen Hu. SceneTracker: Long-term scene flow estimation network. *IEEE Transactions on Pattern Analysis and Machine Intelligence*, 2025.

[71] Jianyuan Wang, Minghao Chen, Nikita Karaev, Andrea Vedaldi, Christian Rupprecht, and David Novotny. VGGT: Visual geometry grounded transformer. In *Proceedings of the Computer Vision and Pattern Recognition Conference*, pages 5294–5306, 2025.

[72] Shuzhe Wang, Vincent Leroy, Yohann Cabon, Boris Chidlovskii, and Jerome Revaud. DUSt3R: Geometric 3D vision made easy. In *Proceedings of the IEEE/CVF conference on computer vision and pattern recognition*, pages 20697–20709, 2024.

[73] Wenshan Wang, Delong Zhu, Xiangwei Wang, Yaoyu Hu, Yuheng Qiu, Chen Wang, Yafei Hu, Ashish Kapoor, and Sebastian Scherer. TartanAir: A dataset to push the limits of visual SLAM. In *2020 IEEE/RSJ International Conference on Intelligent Robots and Systems (IROS)*, pages 4909–4916. IEEE, 2020.

[74] Hongchi Xia, Yang Fu, Sifei Liu, and Xiaolong Wang. RGBD objects in the wild: Scaling real-world 3D object learning from RGB-D videos. In *Proceedings of the IEEE/CVF Conference on Computer Vision and Pattern Recognition*, pages 22378–22389, 2024.

[75] Yuxi Xiao, Qianqian Wang, Shangzhan Zhang, Nan Xue, Sida Peng, Yujun Shen, and Xiaowei Zhou. SpatialTracker: Tracking any 2D pixels in 3D space. In *Proceedings of the IEEE/CVF Conference on Computer Vision and Pattern Recognition*, pages 20406–20417, 2024.

[76] Yuxi Xiao, Jianyuan Wang, Nan Xue, Nikita Karaev, Yuri Makarov, Bingyi Kang, Xing Zhu, Hujun Bao, Yujun Shen, and Xiaowei Zhou. SpatialTrackerV2: 3D point tracking made easy. *arXiv preprint arXiv:2507.12462*, 2025.

[77] Jinbo Xing, Menghan Xia, Yong Zhang, Haoxin Chen, Wangbo Yu, Hanyuan Liu, Gongye Liu, Xintao Wang, Ying Shan, and Tien-Tsin Wong. DynamiCrafter: Animating open-domain images with video diffusion priors. In *European Conference on Computer Vision*, pages 399–417. Springer, 2024.

[78] Tian-Xing Xu, Xiangjun Gao, Wenbo Hu, Xiaoyu Li, Song-Hai Zhang, and Ying Shan. GeometryCrafter: Consistent geometry estimation for open-world videos with diffusion priors. In *Proceedings of the IEEE/CVF International Conference on Computer Vision*, pages 6632–6644, 2025.

[79] Jianing Yang, Alexander Sax, Kevin J Liang, Mikael Henaff, Hao Tang, Ang Cao, Joyce Chai, Franziska Meier, and Matt Feiszli. Fast3R: Towards 3D reconstruction of 1000+ images in one forward pass. In *Proceedings of the Computer Vision and Pattern Recognition Conference*, pages 21924–21935, 2025.

[80] Lihe Yang, Bingyi Kang, Zilong Huang, Zhen Zhao, Xiaogang Xu, Jiashi Feng, and Hengshuang Zhao. Depth Anything V2. *Advances in Neural Information Processing Systems*, 37:21875–21911, 2024.

[81] Zhuoyi Yang, Jiayan Teng, Wendi Zheng, Ming Ding, Shiyu Huang, Jiazheng Xu, Yuanming Yang, Wenyi Hong, Xiaohan Zhang, Guanyu Feng, et al. CogVideoX: Text-to-video diffusion models with an expert transformer. *arXiv preprint arXiv:2408.06072*, 2024.

[82] Yao Yao, Zixin Luo, Shiwei Li, Jingyang Zhang, Yufan Ren, Lei Zhou, Tian Fang, and Long Quan. BlendedMVS: A large-scale dataset for generalized multi-view stereo networks. In *Proceedings of the IEEE/CVF conference on computer vision and pattern recognition*, pages 1790–1799, 2020.

[83] Chandan Yeshwanth, Yueh-Cheng Liu, Matthias Nießner, and Angela Dai. ScanNet++: A high-fidelity dataset of 3D indoor scenes. In *Proceedings of the IEEE/CVF International Conference on Computer Vision*, pages 12–22, 2023.

[84] Bowei Zhang, Lei Ke, Adam W. Harley, and Katerina Fragkiadaki. TAPIP3D: Tracking any point in persistent 3D geometry. *arXiv preprint arXiv:2504.14717*, 2025.

[85] Hongfei Zhang, Harold Haodong Chen, Chenfei Liao, Jing He, Zixin Zhang, Haodong Li, Yihao Liang, Kanghao Chen, Bin Ren, Xu Zheng, et al. DVD: Deterministic video depth estimation with generative priors. *arXiv preprint arXiv:2603.12250*, 2026.

[86] Yang Zheng, Adam W Harley, Bokui Shen, Gordon Wetzstein, and Leonidas J. Guibas. PointOdyssey: A large-scale synthetic dataset for long-term point tracking. In *Proceedings of the IEEE/CVF International Conference on Computer Vision*, pages 19855–19865, 2023.

[87] Ruijie Zhu, Jiahao Lu, Wenbo Hu, Xiaoguang Han, Jianfei Cai, Ying Shan, and Chuanxia Zheng. MotionCrafter: Dense geometry and motion reconstruction with a 4D VAE. *arXiv preprint arXiv:2602.08961*, 2026.

This appendix complements the main paper with the following:

- Sec. A: Additional details on the training dataset.
- Sec. B: Comparison with a dense 2D tracker [20].
- Sec. C: Comparison with sparse 3D trackers [76, 84].
- Sec. D: Comparison with V-DPM [65].
- Sec. E: Attention visualizations.
- Sec. F: Additional qualitative results.
- Sec. G: Limitations and future work.

A Training Datasets

As summarized in Tab. 7, we train TrackCraft3R on four synthetic datasets: Kubric [16], DynamicReplica [32], PointOdyssey [86], and TartanAir [73]. Kubric, DynamicReplica, and PointOdyssey provide RGB, depth, camera parameters, and 3D trajectories. For Kubric [16], following [13], we render 6K sequences (480×832, 81 frames) and extract dense trajectories from the first frame. DynamicReplica and PointOdyssey provide sparse 3D trajectories from mesh vertices. TartanAir contains static scenes with large camera motion and provides RGB, depth, and camera poses. During training, we randomly sample a temporal stride from the strides listed in Tab. 7 for each dataset to cover diverse motion patterns.

Table 7: **Training data.** Number of videos and temporal strides.

Dataset	#Videos	Strides
Kubric [16]	6,042	[3, 4, 5, 6, 7]
DynamicReplica [32]	483	[5, 6, 7, 8, 9]
PointOdyssey [86]	45	[2, 3, 4, 5, 6]
TartanAir [73]	163	[1, 2, 3]

B Comparison with Lifted Dense 2D Tracker

Table 8: **3D tracking comparison with lifted AllTracker [20].** We report AJ, APD_{3D}, and OA after Sim(3) alignment. The estimated dense 2D tracks from AllTracker are lifted to 3D using ViPE [25] depth and camera poses. The best and second-best results are highlighted in dark and light blue, respectively.

	ADT [56]			PStudio [31]			DR [32]			PO [86]			Kubric [16]			Average		
Method	AJ↑	APD_{3D}↑	OA↑	AJ↑	APD_{3D}↑	OA↑	AJ↑	APD_{3D}↑	OA↑	AJ↑	APD_{3D}↑	OA↑	AJ↑	APD_{3D}↑	OA↑	AJ↑	APD_{3D}↑	OA↑
AllTracker [20] + ViPE [25]	0.6177	0.7234	0.9421	0.6463	0.8214	0.8301	0.4719	0.5979	0.9123	0.5410	0.7098	0.8601	0.2903	0.3879	0.9318	0.5134	0.6481	0.8953
TrackCraft3R + ViPE [25]	0.6683	0.7688	0.9405	0.6803	0.8163	0.8937	0.5842	0.7034	0.9408	0.5836	0.7262	0.8943	0.3032	0.3940	0.9597	0.5639	0.6817	0.9258

In Tab. 8, we further compare TrackCraft3R with AllTracker [20], a recent dense 2D tracker, on sparse and dense 3D tracking benchmarks. We use depth and camera pose from ViPE [25] to unproject the estimated 2D tracks into 3D world coordinates. TrackCraft3R consistently outperforms AllTracker, achieving higher overall AJ, APD_{3D}, and OA across all benchmarks.

C Comparison with Sparse 3D Trackers

Table 9: **3D tracking comparison with SpatialTrackerV2 [76] and TAPIP3D [84].** We report AJ, APD_{3D}, and OA after Sim(3) alignment. The best and second-best results are highlighted in dark and light blue, respectively.

	ADT [56]			PStudio [31]			DR [32]			PO [86]			Average		
Method	AJ↑	APD_{3D}↑	OA↑	AJ↑	APD_{3D}↑	OA↑	AJ↑	APD_{3D}↑	OA↑	AJ↑	APD_{3D}↑	OA↑	AJ↑	APD_{3D}↑	OA↑
SpatialTrackerV2 [76] + ViPE [25]	0.6533	0.7818	0.9193	0.6152	0.7961	0.8142	0.4499	0.5762	0.9172	0.5023	0.7060	0.8042	0.5552	0.7150	0.8637
TAPIP3D [84] + ViPE [25]	0.6616	0.7602	0.9419	0.6426	0.8224	0.8248	0.4131	0.5925	0.7586	0.5487	0.7055	0.8698	0.5665	0.7202	0.8488
TrackCraft3R + ViPE [25]	0.6683	0.7688	0.9405	0.6803	0.8163	0.8937	0.5842	0.7034	0.9408	0.5836	0.7262	0.8943	0.6291	0.7537	0.9173

In Tab. 9, we compare TrackCraft3R with the recent sparse 3D trackers SpatialTrackerV2 [76] and TAPIP3D [84] on the sparse 3D tracking benchmarks. Note that SpatialTrackerV2 and TAPIP3D also take camera poses and depth from off-the-shelf models as input. For fair comparison, we use ViPE [25] for all methods. TrackCraft3R outperforms both SpatialTrackerV2 and TAPIP3D, achieving the best average AJ, APD_{3D}, and OA.

Table 10: **3D tracking comparison with V-DPM [65].** We report AJ, APD_{3D}, and OA after Sim(3) alignment. The best and second-best results are highlighted in dark and light blue, respectively.

Method	ADT [56]			PStudio [31]			DR [32]			PO [86]			Average		
	AJ↑	APD_{3D}↑	OA↑	AJ↑	APD_{3D}↑	OA↑	AJ↑	APD_{3D}↑	OA↑	AJ↑	APD_{3D}↑	OA↑	AJ↑	APD_{3D}↑	OA↑
V-DPM [65]	0.7745	0.9126	0.8668	0.8501	0.9606	0.9065	0.6041	0.8319	0.7670	0.7030	0.9567	0.7785	0.7329	0.9155	0.8297
TrackCraft3R + DA3 [46]	0.8040	0.8692	0.9701	0.8190	0.9036	0.9454	0.6575	0.7614	0.9742	0.6835	0.7902	0.9227	0.7410	0.8311	0.9531
TrackCraft3R + V-DPM [65]	0.8418	0.9183	0.9477	0.7518	0.8607	0.9227	0.7128	0.8150	0.9626	0.8146	0.9386	0.9008	0.7803	0.8832	0.9335

D Comparison with V-DPM

While V-DPM [65] is a concurrent work trained on different dataset scales, we provide additional comparisons for completeness. Tab. 10 reports AJ, APD_{3D}, and OA on sparse tracking benchmarks, evaluated on the first 24 frames. We also report TrackCraft3R + V-DPM, which uses V-DPM's predicted frame-anchored reconstruction pointmaps as our input geometry. Both TrackCraft3R + DA3 [46] and TrackCraft3R + V-DPM outperform V-DPM in AJ and OA, while V-DPM achieves slightly higher APD_{3D}. Notably, TrackCraft3R runs **6.6× faster** with **2.3× less memory** than V-DPM (Tab. 11). Below, we provide a detailed discussion of TrackCraft3R *vs.* V-DPM.

Dataset Scale. V-DPM relies heavily on 3D/4D supervision throughout its training. Its backbone (VGGT [71]) is pre-trained on 17 3D-annotated datasets: Co3Dv2 [58], BlendedMVS [82], DL3DV [47], MegaDepth [43], Kubric [16], WildRGB [74], ScanNet [8], HyperSim [59], Mapillary [1], Habitat [67], Replica [32], MVS-Synth [26], PointOdyssey [86], Virtual KITTI [4], Aria Synthetic Environments [56], Aria Digital Twin [56], and an Objaverse [9]-like synthetic asset set, all providing ground-truth cameras, depths, and pointmaps. V-DPM then fine-tunes both the backbone and geometry/tracking heads on 6 additional 3D/4D-annotated datasets: ScanNet++ [83] and BlendedMVS [82] for static scenes, and Kubric-F [16], Kubric-G [16], PointOdyssey [86], and Waymo [66] for dynamic scenes. The heads use the representations from the pre-trained VGGT [71] backbone and are further fine-tuned, so they ultimately benefit from 23 datasets in total.

In contrast, TrackCraft3R is initialized from Wan2.1-T2V [69], a video diffusion transformer pre-trained on billions of generic web images and videos with *no 3D annotations of any kind*, and fine-tuned on only 4 synthetic 3D/4D datasets (Kubric [16], PointOdyssey [86], and Dynamic Replica [32] for dynamic scenes, and TartanAir [73] for static scenes). **The 3D/4D supervision seen by TrackCraft3R during training is thus a small fraction of that seen by V-DPM (23 datasets *vs.* 4 datasets).**

Despite the dataset scale gap, TrackCraft3R + V-DPM achieves competitive APD_{3D}, while exceeding it in AJ. This demonstrates that the spatio-temporal priors learned from large-scale generic video data effectively compensate for the absence of dense 3D supervision, serving as a strong foundation for 3D tracking. We attribute the small remaining gap to the dataset-scale difference. Even when we use frame-anchored reconstruction maps from V-DPM as input, we only access its 3D point predictions, not its pre-trained representations, while V-DPM's tracking head starts from pre-trained representations trained on 17 datasets. Furthermore, we anticipate that with access to stronger 3D foundation models in the future, TrackCraft3R can achieve even better performance.

Inference Efficiency. TrackCraft3R is substantially more efficient than V-DPM. As shown in Tab. 11, evaluated at 448×448 resolution on 12- and 23-frame clips using a single A6000 GPU, the efficiency gap widens as the clip length L grows. For a 12-frame clip, TrackCraft3R runs **3.2× faster** and uses **1.7× less memory**. For a 23-frame clip, the gap widens to **6.6× faster** and **2.3× less memory**.

Table 11: **Inference efficiency** with different frame lengths.

Frames	Method	Time (s)↓	Memory (GB)↓
12	V-DPM [65]	12.32	12.60
12	**TrackCraft3R**	**3.91**	**7.63**
23	V-DPM [65]	51.49	17.69
23	**TrackCraft3R**	**7.84**	**7.63**

V-DPM predicts track pointmaps $\{P_0(t_j)\}_{j=0}^{L-1}$ via an attention-based, time-conditioned decoder invoked once per timestamp t_j. Running the decoder L times, with each call performing self-attention over all L frames, incurs $\mathcal{O}(L^2)$ time and $\mathcal{O}(L)$ memory. In contrast, TrackCraft3R predicts all trajectories in a *single feed-forward* pass within the *compressed latent space* of a video DiT. For longer clips, TrackCraft3R uses interleaved inference with a fixed clip length, yielding $\mathcal{O}(L)$ runtime and $\mathcal{O}(1)$ peak memory. This efficiency gap is decisive for long-video applications.

Summary. TrackCraft3R trades a small amount of point accuracy for (i) data efficiency, requiring only 4 synthetic 3D/4D-annotated datasets for fine-tuning compared to V-DPM's 23 3D/4D-annotated datasets; (ii) compatibility with any 3D geometry estimator, naturally benefiting from future advances in 3D foundation models, including V-DPM itself; and (iii) substantial efficiency gains, particularly for long videos.

E Additional Attention Visualization

Temporal alignment between track and geometry latents. Fig. 6 and Fig. 7 visualize the query–key attention from a track latent $\mathbf{r}_5$ to geometry latents $\{\mathbf{g}_k\}_{k=0}^{F}$ across transformer layers. The red box marks the temporally aligned geometry latent $\mathbf{g}_5$. We observe that each track latent $\mathbf{r}_i$ assigns the highest attention to its corresponding geometry latent $\mathbf{g}_i$. We quantify this by averaging attention mass over all transformer layers: the temporally aligned geometry latent receives the highest attention (29.0% in Fig. 6 and 30.1% in Fig. 7). This verifies that temporal RoPE alignment provides a reliable signal for identifying the correct timestamp.

Correspondence within aligned latents. Fig. 8 and Fig. 9 visualize attention between $\mathbf{r}_5$ and $\mathbf{g}_5$ across transformer layers. Full 3D attention establishes reliable spatial correspondences between track and geometry latents under motion (*e.g.*, the moving baseball in Fig. 8). As discussed in prior works [53, 63], we observe layer-wise behaviors: several layers focus on RoPE-initialized positions, while a subset of layers (highlighted in red) finds correspondences between the same physical points. The same layers exhibit this behavior across different samples (Fig. 9), indicating that these layer-wise functions are consistent across inputs.

F Additional Qualitative Results

We present additional qualitative results and comparisons with DELTAv2 [55] on ITTO [10] and DAVIS [57] videos in Figs. 10 and 11.

G Limitations and Future Work

Following the common convention in world-coordinate 3D point tracking [54, 55, 76, 84], TrackCraft3R relies on per-frame depth and camera pose from external 3D foundation models [25, 44, 46, 71]. While this design choice aligns with prior work, it also means that the accuracy of TrackCraft3R is bounded by the quality of the input geometry, as shown in Tab. 4 in the main paper. At the same time, this design allows TrackCraft3R to benefit from future advances in 3D foundation models, as improved geometry estimators can be incorporated without retraining.

A further direction is to jointly generate video and 3D tracks, unifying generation and dense 4D perception within a single video DiT. Such a unified model could serve as a strong foundation for robotic manipulation, where recent work uses generated videos and tracks as intermediate representations for action prediction [2, 27, 38, 39].

Our method may have implications when applied to real-world videos involving people, such as tracking individuals. We encourage responsible use.

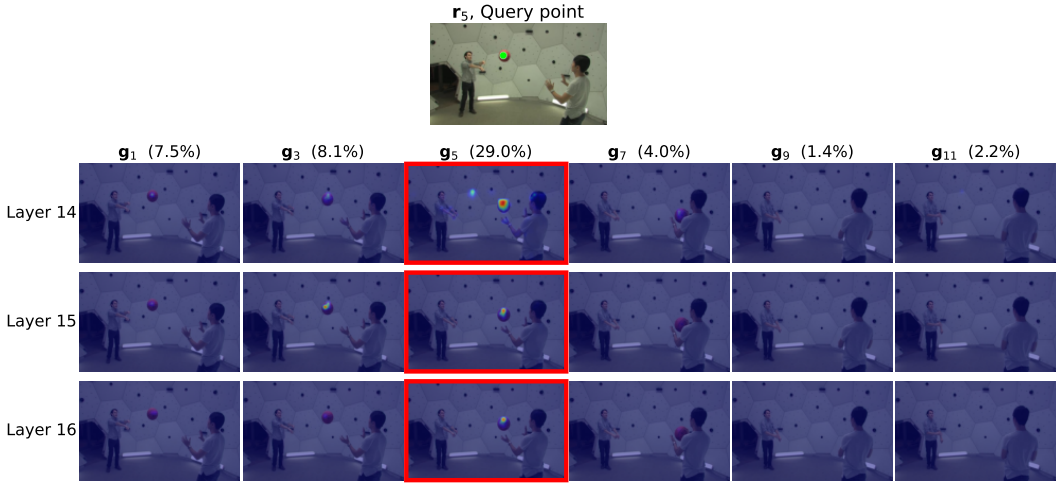

Figure 6: **Query–key attention visualization on PStudio [31].** The query point is marked with a green circle on the baseball. We visualize attention from the track latent $\mathbf{r}_5$ at timestamp t_5 to geometry latents $\{\mathbf{g}_j\}_{j=0}^{F}$ across transformer layers. Attention is concentrated on the temporally aligned geometry latent $\mathbf{g}_5$ (29.0%), showing that RoPE correctly assigns a target timestamp to each track latent.

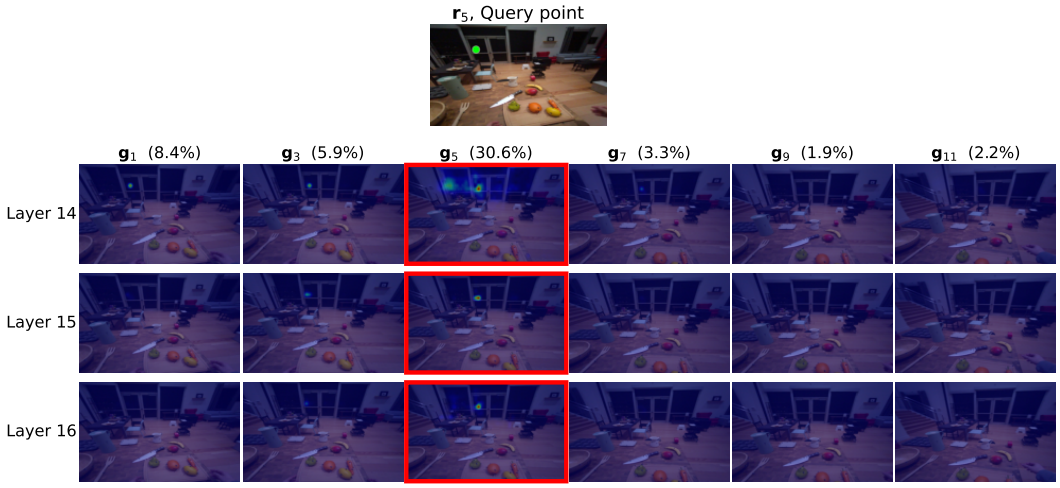

Figure 7: **Query–key attention visualization on ADT [56].** The query point is marked with a green circle on the left door. We visualize attention from the track latent $\mathbf{r}_5$ at timestamp t_5 to geometry latents $\{\mathbf{g}_j\}_{j=0}^{F}$ across transformer layers. Attention is concentrated on the temporally aligned geometry latent $\mathbf{g}_5$ (30.6%), showing that RoPE correctly assigns a target timestamp to each track latent.

s

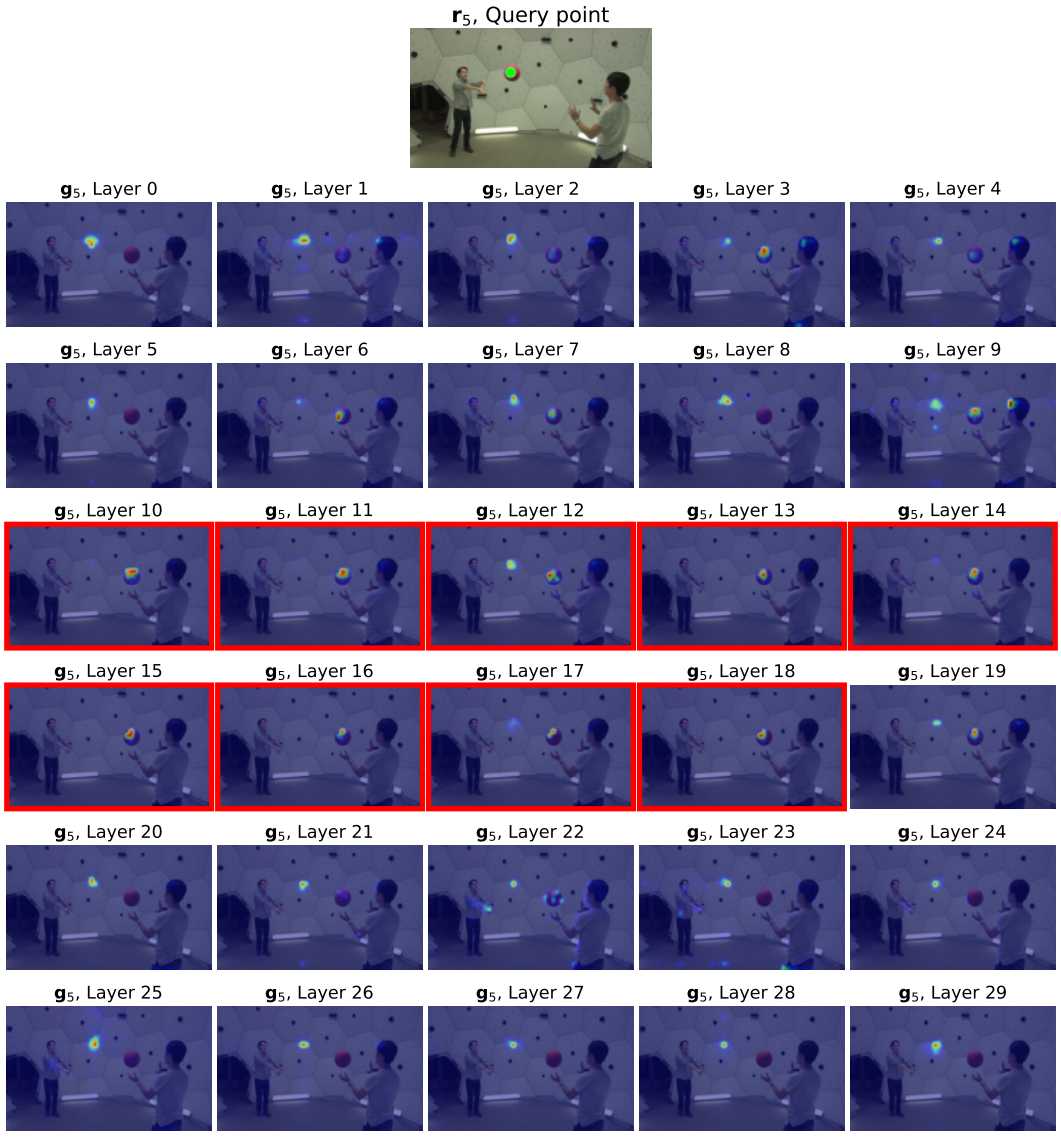

Figure 8: **Query–key attention visualization on PStudio [31].** The query point is marked with a green circle. Attention between the temporally aligned track and geometry latents identifies accurate correspondences of the same physical points in specific layers (highlighted in red boxes).

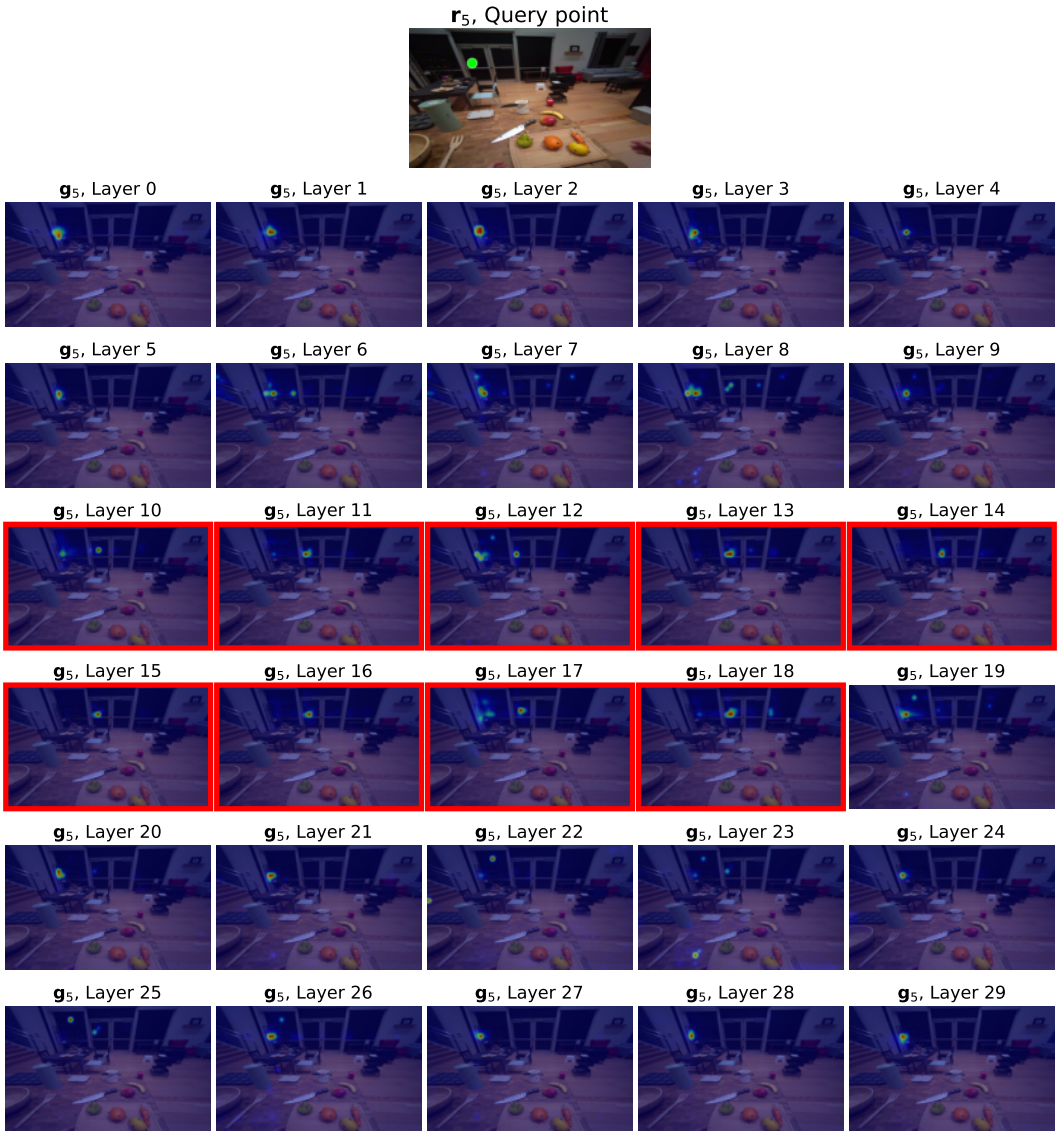

Figure 9: **Query–key attention visualization on ADT [56].** The query point is marked with a green circle. Attention between the temporally aligned track and geometry latents identifies accurate correspondences of the same physical points in specific layers (highlighted in red boxes).

Figure 10: **Qualitative results on ITTO [10] videos.** TrackCraft3R accurately estimates dense 3D trajectories on real-world videos under large camera motion, object dynamics and occlusion.

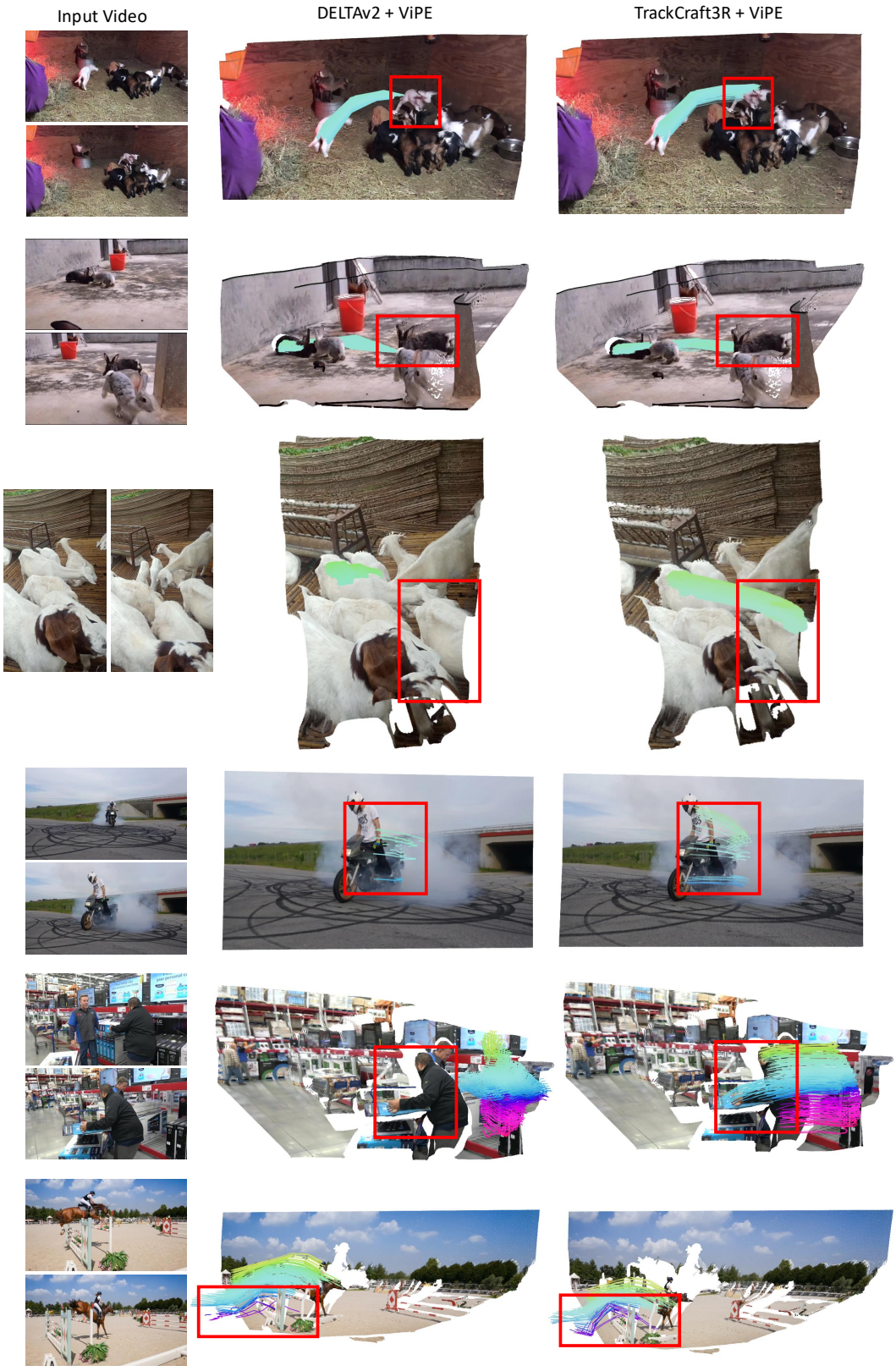

Figure 11: **Qualitative comparison on ITTO [10] and DAVIS [57] videos.** TrackCraft3R accurately estimates dense 3D trajectories on real-world videos under large camera motion, object motion, and occlusion. Note that the same query points are shared across methods.